Modeling of Magnetorheological Fluids by the Discrete Element Method

Mickaël Kargulewicz

Ivan Iordanoff

Arts et Métiers ParisTech,
Institut de Méchanique et Ingénierie - Bordeaux
(UMR 5295),
Esplanade des Arts et Métiers,
33405, Talence Cedex, France

Victor Marrero

John Tichy[1]
e-mail: tichyj@rpi.edu

Department of Mechanical, Aerospace, and
Nuclear Engineering,
Rensselaer Polytechnic Institute,
Troy, NY 12180-3590

Magnetorheological (MR) fluids are fluids whose properties vary in response to an applied magnetic field. Such fluids are typically composed of microscopic iron particles ($\sim 1-20\ \mu m$ diameter, $20-40\%$ by volume) suspended in a carrier fluid such as mineral oil or water. MR fluids are increasingly proposed for use in various mechanical system applications, many of which fall in the domain of tribology, such as smart dampers and clutches, prosthetic articulations, and controllable polishing fluids. The goal of this study is to present an overview of the topic to the tribology audience, and to develop an MR fluid model from the microscopic point of view using the discrete element method (DEM), with a long range objective to better optimize and understand MR fluid behavior in such tribological applications. As in most DEM studies, inter-particle forces are determined by a force-displacement law and trajectories are calculated using Newton's second law. In this study, particle magnetization and magnetic interactions between particles have been added to the discrete element code. The global behavior of the MR fluid can be analyzed by examining the time evolution of the ensemble of particles. Microscopically, the known behavior is observed: particles align themselves with the external magnetic field. Macroscopically, averaging over a number of particles and a significant time interval, effective viscosity increases significantly when an external magnetic field is applied. These preliminary results would appear to establish that the DEM is a promising method to study MR fluids at the microscopic and macroscopic scales as an aid to tribological design. [DOI: 10.1115/1.4006021]

Keywords: magnetism, lubrication, hydrodynamic, rheology, non-Newtonian

1 Introduction

Magnetorheological (MR) fluids have been in existence for many decades, the first US patent being generally attributed to Rabinow in 1947 as discussed by Carlson [1]. Until quite recently, this technology has been called a 'laboratory curiosity,' with descriptions and articles in popular science magazines, but few, if any, actual technical applications. However, in the 1980s, researchers began to develop MR fluids as commercial products, and since that time devices using this technology have increasingly been put into use.

The most common tribology-based application has been the 'smart damper' in vehicles [2], or building systems [3], as well as idealized control system devices [4]. The basic principle of use is by changing the effective viscosity of the damping fluid, the damping coefficient can be changed, and thus the system behavior optimized. Other applications are smart clutches whose power transmissibility can be changed rapidly in response to operating conditions [5], and smart brakes [6]. There has recently been considerable interest in the use of magnetorheological fluids for prosthetic joints [7,8] and even limbs [9] for the case of severely injured patients. There has been a recent explosion of literature on MR applications; thus the set of articles cited is by no means comprehensive. Likewise, there are many other applications that have little if anything to do with tribology such as haptics (tactile feedback technology such as for surgical training devices); and bullet resistant vests which can change from soft and flexible for normal conditions, to rigid in dangerous situations.

Magnetic fluids can be loosely categorized as MR fluids and ferro fluids. Both contain ferromagnetic particles, but ferro fluid particles are in the nanometer range (3–15 nm) while MR fluid particles are of micrometer size (1–20 μm). In MR fluids, the magnetic moment of the particles is induced, while in ferro fluids the magnetic moment is permanent. The latter are influenced by Brownian motion, do not tend to agglomerate or form chains, and do not tend to settle due to gravity. In MR fluids, additives to promote particle suspension are usually present in small amounts.

The basic phenomena in magnetorheology are related to controlling the structure and properties of a fluid-particle mixture by applying a magnetic field. The applied field polarizes the ferro magnetic particles of the MR fluid, and thus induces a chainlike agglomeration of particles in the direction of the magnetization and gives rise to a significant effective viscosity increase. The magnetic moment of particles is induced by the applied field and the process of effective viscosity change is largely reversible.

A goal of the present paper is to propose a model for MR fluids using the discrete element method (DEM) [10,11]. DEM is a method for computing the motion of a large number of particles. It is related to molecular dynamics but generally differentiated by the size of the particles being larger. Large particles mean that Brownian motion is not included, the particles have more inertia and are likely to collide with one another, and angular momentum of the particles may need to be considered.

Researchers have far more extensively studied an electrical analog to MR fluids, namely, electrorheological (ER) fluids, generally attributed first to Winslow in 1949 [12]. These fluids are well described in the review article of Halsey [13]. A considerable number of papers in the literature can be found on experiments and simulation of the properties of ER fluids [14–19]. In many ways the theoretical methodology of these papers is very similar to that used here, but there are key differences to be discussed below. Likewise, the global behavior between ER and MR fluids exhibits key differences - both the model predictions and experimentally determined behavior. An experimental and theoretical

[1]Corresponding author.

Contributed by the Tribology Division of ASME for publication in the JOURNAL OF TRIBOLOGY. Manuscript received April 20, 2011; final manuscript received December 20, 2011; published online June 26, 2012. Assoc. Editor: George K. Nikas.

paper by Chen et al. from 1995 [20] uses a similar approach, other than, of course, the differences in basic character between electric and ferromagnetic field strengths. Likewise, qualitatively similar macroscopic predictions are obtained.

The behavior of MR and ER fluids is commonly represented as a Bingham fluid as described in the text of Bird et al. [21], Part 1 - Fluid Mechanics. Tichy [22] describes some of the peculiarities of this model in lubrication flow. Bird et al. [21] describe the Bingham fluid as purely viscous (or generalized Newtonian). The shear stress in a given direction on a given surface is linearly dependent on the corresponding rate of strain (as in the Newtonian case), however, there is a yield shear strength which must be overcome by the magnitude of the extra stress tensor before flow begins. In the case of MR fluids, this yield strength parameter depends on the magnitude of the magnetic field.

The reader is referred to the work of Rankin et al. [23] for a comprehensive discussion of the differences between MR and ER fluids. MR fluids can exhibit field-induced shear of two orders of magnitude larger than the ER fluids, which makes them more promising for many applications. On the other hand, the relatively large particle size and the high particle density make settling of the particles an impediment to many possible applications. From a modeling point of view, the nature of the field strengths in MR and ER fluids are quite different. It is convenient to divide MR fluids in three regimes of applied field strength. At low fields the particle magnetization is linear and the calculation of forces is analogous that of ER fluids. At the other extreme, the magnetization is fully saturated, and the particles are simple dipoles of constant strength. There is also, of course, an intermediate region merging linearity to full saturation. The proposed DEM model presented in this paper can be applied to MR fluids for the three regimes of applied field strength.

Just as the literature on applications has grown immensely in recent years, papers on the fundamentals of MR fluids have appeared with increasing frequency, although lagging in number far behind ER fluid papers. Some recent papers in several subcategories are mentioned briefly below to give the reader an idea as to the nature of the field. However, this is not intended to be a comprehensive bibliography. In the case of experimental papers, de Vicente et al. [24] examine the effect of field strengthon flow behavior - the competition between viscous and magnetization effects. Field strength is described through the so-called Mason number *Ma* (see below), a ratio of viscous shear stress to effective magnetic stress (proportional to the square of the magnetization). Genç and Phulé [25] experimentally examine the effect of different size iron particles. The effect of surface forces and surface-active additives is examined by Klingenberg et al. [26]. Clarcq et al. [27] conducted rheological experiments in dynamic mode at very low strain to understand the influence of the structure on MR rheology.

There is a considerable number of modeling papers in the literature which investigate the behavior of MR fluids from a microstructural perspective. The vast majority of such papers seem to take the approach well-described in Bird et al. [28], Part 2-Kinetic Theory, and Larson [29]. Very briefly, the idea is to idealize the non-Newtonian fluid as a Newtonian fluid solvent with a solute microstructure. The microstructure generally consists of particles (beads) possibly connected by rods or springs, subject to forces and torques. The motion of these particles through an idealized surface within the fluid causes a momentum flux at the microscale, which is interpreted as a stress at the continuum scale. A set of coordinate values (*e.g.*, bead position and spring orientation) describes the system configuration. Typically, a distribution function is assumed for the configuration of the beads, and the global stress is the integral of the local momentum times the distribution function over all possible configurations. One might call these distributed microstructural models, as opposed to discrete models which track the course of all individual particles.

In this fashion, Yi et al. [30] assume that the particles are magnetic dipoles aligned in straight chains across a shearing gap, and calculate a yield strength assuming a normal distribution of chain angles. The forces on the particles are determined from the classical electrodynamics equations for force on an independent magnetic dipole in a magnetic field. Furst and Gast [31] previously applied the same general technique but used the force to shear a chain of particles. The model of Jang et al. [32] uses a more sophisticated approach to calculating the interparticle forces, based on a lattice model of the magnetic particles. Ginder and Davis [33] calculated the interparticle forces and resulting shear stresses in a MR fluid using a finite-element technique. The MR fluid was modeled by infinite chains of spherical and magnetizable particles aligned with a magnetic induction field. The study found that the maximum shear strength of the MR fluid varies as the square of the saturation magnetization of the particles, revealing a near independence of the stress on the magnetic induction at saturation.

In classifying the models of MR fluids, the distinguishing feature is not continuum versus microscale - virtually all models other than Bingham deal with the microscale. The distinction is rather: are the microscale models distributed or discrete. The present literature investigation found far more models of the distributed type just described and relatively fewer DEM. Kroger et al. [34] use a molecular dynamics approach to ferro fluids with nanoscale particles, and a simple model of perfectly oriented particles in the case of MR fluids without particle contact. In the closest to the present study, a modified DEM method is used by Han et al. [35]. They use a system of linear equations to account for the magnetization of individual particles inthe presence of a uniform field. They find visualizations similar to those of the present study, but the predicted flow curves show a much more gradual trend than the Bingham model. Finally, Melle et al. [36] use two-dimensional discrete simulations neglecting particle inertia. They find results similar to experiments in predicting the number of particles in chains, but do not produce stress-strain rate curves.

In this Introduction, some pertinent literature and background have been discussed. In the next section, a description of typical MR fluids and their behavior is presented and the discrete element model of this study is examined. In Sec. 3, the present DEM method is described. In Sec. 4, the simulations are discussed and results presented, and conclusions presented in Sec. 5. As in the case of many existing papers, we concentrate on conditions approaching saturation magnetization, which produces off/on behavior at low to moderate rates of shear.

2 MR Fluid Behavior

MR Fluids are composed of a high concentration of magnetizable particles dispersed in a nonmagnetic carrier fluid. MR fluid particle sizes typically range from 1–20 μm. Carrier fluids are selected based on their viscosity, their temperature stability, and their compatibility with other materials of the device. The most common carrier fluids are hydrocarbon oils, silicon oils or simply water. Additives have many purposes such as to inhibit particle settling and agglomeration, reduce friction and prevent particle oxidation.

The significant difference between iron particle density ($\rho_p \sim 7.5$ g/cm^3) and carrier fluid density ($\rho_f \sim 1$ g/cm^3) makes MR fluids susceptible to long-term separation. This phenomenon may be accompanied by particle agglomeration, which means that particles stick together in the absence of a magnetic field (due; for example, to a small level of remnant magnetization in the particles). Additives improve stability and durability of MR fluids, which is crucial in industrial applications.

Particles need to be ferromagnetic in order to be magnetizable when a magnetic field is applied. When a ferromagnetic material is placed in a magnetic field, each atom will behave as a magnet and change its orientation following the magnetic field direction. MR fluid particles are primarily of micrometer scale and are too massive for Brownian motion to keep them suspended.

MR fluids respond to magnetic fields with a dramatic change in rheological behavior. The fluid can rapidly and reversibly change

from a free-flowing liquid to a semisolid with controllable yield strength when exposed to a magnetic field. When a magnetic field is applied to MR fluids, particles in suspension move to form chains parallel to the magnetic field. In the absence of magnetic field, the particle distribution is random and homogeneous, Fig. 1(*a*) (upper left). When an external magnetic field **H** is applied in the direction across the film, the ferromagnetic particles acquire a dipole moment **m**, and the particles attract one another, Fig. 1(*b*) (upper right). In the absence of shearing, stable chains form across the film, Fig. 1(*c*) (middle left). In the presence of a surface shear velocity **V**, the chains deform in shear, Fig. 1(*d*) (middle right); eventually resulting in rupture, Fig. 1(*e*) (lower left). During shear, the process of formation and rupture of chains is ongoing, causing a significant increase in effective viscosity relative to that of the carrier fluid. If the magnetization is removed, the particles essentially move in the shearing direction, but with a random component due to inter particle collisions and collisions with the bounding wall, Fig. 1(*f*) (lower right). The process of applying and removing the magnetic field is nearly reversible.

The model most commonly used to portray global MR fluid continuum behavior is the so-called Bingham model, which can be mathematically described by:

$$\dot{\gamma}_{kl} = \frac{\partial v_k}{\partial x_l} + \frac{\partial v_l}{\partial x_k}, \quad \dot{\gamma} = \sqrt{\frac{1}{2}\sum_{m=1}^{3}\sum_{n=1}^{3}\dot{\gamma}_{mn}\,\dot{\gamma}_{nm}}, \qquad (1)$$

$$\tau = \sqrt{\frac{1}{2}\sum_{m=1}^{3}\sum_{n=1}^{3}\tau_{mn}\tau_{nm}}$$

$$\tau \le \tau_0 : \eta = \infty, \quad \tau > \tau_0 : \eta = \eta_0 + \frac{\tau_0}{\dot{\gamma}}, \quad \tau_{kl} = \eta\ \dot{\gamma}_{kl} \qquad (2)$$

The symbols used are listed in the Nomenclature. In this complete formulation of the model (not just in the case of simple uniform shear), $\dot{\gamma}$ and τ are the magnitudes (second invariants) of the rate-of-strain and deviatoric stress tensors, respectively. If the intensity of the stress state τ is less than a 'yield stress' material parameter τ_0, the material is essentially rigid, *i.e.*, the viscosity is infinite, $\eta = \infty$. If the stress exceeds the yield stress, the fluid flows in a quasi-Newtonian manner with the viscosity η as shown. In simple shearing flow the Bingham model simplifies to:

$$v_x = v_x(z), \quad \dot{\gamma}_{zx} = \frac{dv_x}{dz}, \quad \tau_{zx} = \frac{F_x}{A_z}, \quad A_z = L_x L_y,$$
$$\tau = |\tau_{zx}|, \quad \gamma = |\dot{\gamma}_{zx}|$$
$$\dot{\tau_{zx}} = \eta(\dot{\gamma})\,\dot{\gamma}_{zx} = \frac{\dot{\gamma}_{zx}}{|\dot{\gamma}_{zx}|}\tau_0 + \eta_0\,\dot{\gamma}_{zx}$$

In the case of MR fluids, the flow threshold $\tau_0 = \tau_0(H_z)$ can be seen at the micro scale as the shear resistance limit of the ensemble particle chains per unit surface area. When $\tau > \tau_0$ chains are constantly in the process of breaking and reorganizing to form new chains. In general, the higher the field intensity (up to saturation), the greater the magnetic forces, and the greater the yield stress. This behavior is portrayed schematically in Fig. 2. However, the behavior in experiments and the results of various models are quite variable. In some cases, the transition from solid-like to fluid-like is far more gradual. In other cases, the transition is sudden at saturation, but more gradual at lower magnetization.

3 DEM Model

Currently, the finite element method is most widely used to study the behavior of mechanical systems, but, this method generally requires a continuum constitutive equation for material behavior and is not normally used to investigate discrete microscopic phenomena. This paper is not the proper forum to evaluate numerical methods, but suffice it to say that DEM is becoming

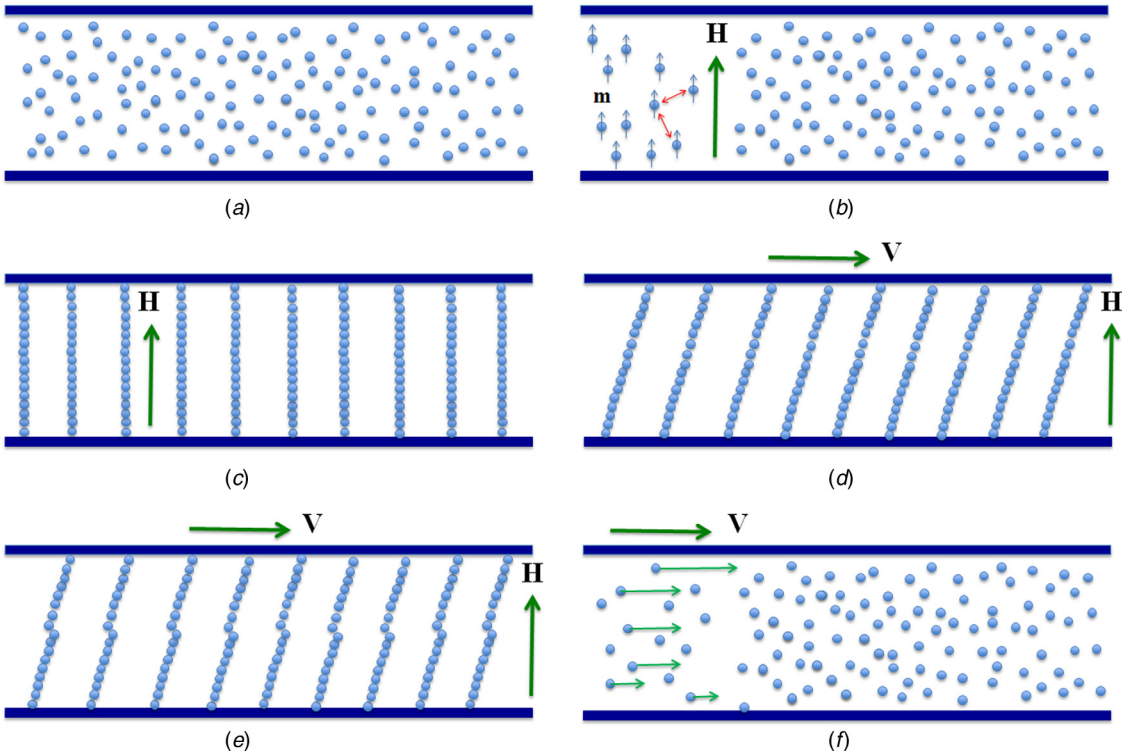

Fig. 1 Particles in MR fluid. (*a*) upper left: no magnetic field, no shear - random distribution; (*b*) upper right: field applied - magnetization of particles, interparticle forces; (*c*) middle left: field applied, formation of chains; (*d*) middle right: shear applied, chains deform; (*e*) lower left: chains rupture in shear; (*f*) lower right: field removed, particles move with shear.

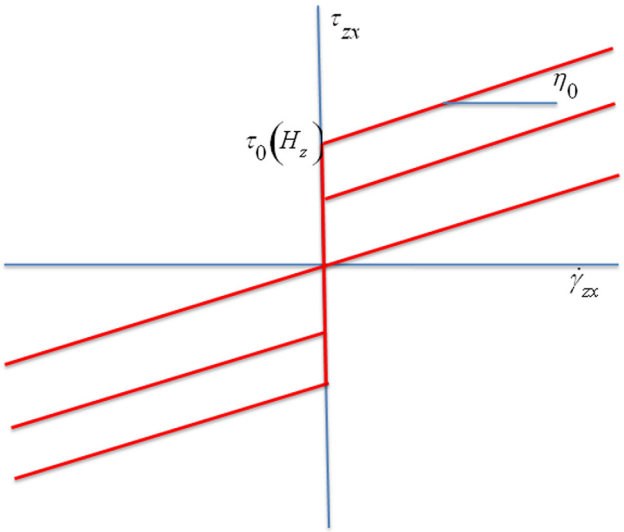

Fig. 2 Schematic of the Bingham Model, yield stress varies with magnetization

widely accepted as an effective method to study discontinuous behavior. As the study of particles in an MR fluid is essentially discontinuous, we have chosen the DEM as a tool for the present study.

The DEM model domain is composed of three layers, see Fig. 3. The first layer is the upper plane wall which is motionless, the second layer is the MR fluid with magnetic spherical particles initially randomly placed therein, and the third layer is the lower wall which slides in its own plane to incorporate the shearing motion. The domain is limited by the two physical walls normal to the z axis, and by two virtual walls normal to the y axis. Boundary conditions are periodic in the x direction in order to mimic an infinite flow field. The walls are likewise composed of slightly larger spheres which facilitate the calculations and could represent the wall roughness. The MR fluid in the middle layer contains a carrier fluid in which the magnetic particles are suspended.

In brief overview, the DEM algorithm works as follows. The starting point is an initial configuration of position $\mathbf{x}_i^p$, velocity $\mathbf{v}_i^p$, and angular velocity ω_i^p, of solid particle i within the carrier fluid. The imposed sliding velocity of the lower surface provides energy and momentum to the system. The forces and moments are summed on each solid particle of the MR fluid domain at time t, yielding the particle linear and angular accelerations. The forces and torques (moments) on the ith particle are due to (1) actual contact between this and another particle: $\mathbf{F}_i^c$ and $\mathbf{T}_i^c$, (2) the viscous fluid: $\mathbf{F}_i^v$ and $\mathbf{T}_i^v$, and (3) magnetism: $\mathbf{F}_i^m$ and $\mathbf{T}_i^m$:

$$\ddot{\mathbf{x}}_i^p = \dot{\mathbf{v}}_i^p = \frac{1}{m_p}(\mathbf{F}_i^c + \mathbf{F}_i^v + \mathbf{F}_i^m), \quad \dot{\omega}_i^p = \frac{1}{I_p}(\mathbf{T}_i^c + \mathbf{T}_i^v + \mathbf{T}_i^m) \tag{4}$$

The volume of a spherical particle is $\mathcal{V}_p = (4/3)\pi R_p^3$, the mass is $m_p = \rho_p \mathcal{V}_p$ and the mass moment of inertia is $I_p = (2/5)m_p R_p^2$. The superscript 'dot' signifies derivative with respect to time. The

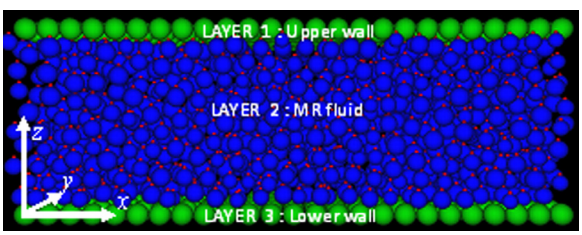

Fig. 3 Domain of the simulations

accelerations are integrated using a standard Verlet algorithm [37] to produce updated velocities and positions at $t + \Delta t$. The contact of the particles of the MR fluid layer with the particles of the wall produces a force with a shear component F_x, which, in turn causes a spatial average shear stress $\bar{\tau}_{zx}$ and an effective viscosity $\bar{\eta}$:

$$\bar{\tau}_{zx} = \frac{F_x}{A_z}, \quad A_z = L_x L_y, \quad \bar{\dot{\gamma}}_{zx} = \frac{V_x}{L_z}, \quad \bar{\eta} = \frac{\bar{\tau}_{zx}}{\bar{\dot{\gamma}}_{zx}} \tag{5}$$

At the beginning of the simulations, the shear stress and viscosity of Eq. (5) vary with time, exhibiting both rapid fluctuations due to particle collisions and a general drift toward a steady state value. After a period of time, spatial and temporal averaged behavior is reached (although fluctuations persist) and the effective viscosity as a function of average rate of shear is determined. Note that this effective viscosity $\bar{\eta}(\bar{\dot{\gamma}})$ is not necessarily exactly the same as the 'true' viscosity of Eq. (2), but this sort of distinction is for formal rheology papers.

The contact forces and the characteristics of the DEM model in dry nonmagnetic conditions have been well described in previous papers such as Refs. [10] and [11] and will be briefly reprised. After the small increment of time in the simulations Δt, the updated particle positions may indicate actual contact interference of particle i with particles j to n_c. The interaction contact forces $\mathbf{F}_{ij}^c$ have components in the normal and tangential directions $\mathbf{e}_{ij}^n$ and $\mathbf{e}_{ij}^t$. The magnitude depends on the interference between two spheres δ multiplied by an elastic stiffness coefficient k, and its rate of change $\dot{\delta}$ multiplied by a damping coefficient. The contact forces and torques are thus:

$$\begin{aligned} F_i^c &= \sum_j^{n_c} \left(F_{ij}^{cn} e_{ij}^n + F_{ij}^{ct} e_{ij}^t\right), \quad F_{ij}^{cn} = -k\delta_{ij} - 2\alpha\sqrt{km_{ij}}\dot{\delta}_{ij}, \\ F_{ij}^{ct} &= \pm C_{fr} F_{ij}^{cn}, \quad T_i^c = \sum_j^{n_c} \left(R_p e_{ij}^n\right) \times \left(F_{ij}^{ct} e_{ij}^t\right) \end{aligned} \tag{6}$$

The value of the coefficient of friction C_{fr} used in the simulations is 0.03, and value of the plus/minus function is determined by the direction of the relative velocities. For simplicity, the stiffness can be thought of as equivalent to the elastic modulus times the particle radius $k = E_Y R_p$. The discrete simulations are dimensionless, and equivalence between them and the continuum model must be established. Within the discrete simulations, a characteristic time scale of the inter-particle contacts is $t_c = R\sqrt{\rho s/E_Y}$ and likewise a contact velocity scale is $R_p/t_c = \sqrt{E_Y/\rho s}$. For the damping term, m_{ij} is an equivalent mass of the contact $= m_i m_j/(m_i + m_j)$ and there is an equivalence between the damping coefficient and the coefficient of restitution C_{res},

$$\exp\left(\frac{-\alpha\pi}{\sqrt{1-\alpha^2}}\right) = C_{res} \tag{7}$$

In these studies the value $\alpha = 0.07$ has been used, which corresponds to $C_{res} \approx 0.8$.

For the present simple shearing flow, with sliding of the lower surface at V_z, the carrier fluid velocity assumed to be given by,

$$\mathbf{v}^f = v_x^f \mathbf{e}_x + v_y^f \mathbf{e}_y + v_z^f \mathbf{e}_z, \quad v_x^f = V_x\left(1 - \frac{z}{L_z}\right), \quad v_y^f = v_z^f = 0 \tag{8}$$

and vorticity (rotation of a fluid element), to be used below, is as shown:

$$\omega^f = \frac{1}{2}(\nabla \times \mathbf{v}^f), \quad \omega_y^f = -\frac{V_x}{L_z}, \quad \omega_x^f = \omega_z^f = 0 \tag{9}$$

The viscous drag force and moment on a particle depend on the relative velocities and rotation between the fluid and the particle and according to Faxen's laws [38] are given by:

$$\mathbf{F}_i^v = 6_{\pi\eta f} R_p \left(\mathbf{v}^f - \mathbf{v}_i^p\right), \mathbf{T}_i^v = 8_{\pi\eta f} R_p^3 \left(\boldsymbol{\omega}^f - \boldsymbol{\omega}_i^p\right) \tag{10}$$

The magnetic forces and torques are calculated as described below. A field strength $\mathbf{H}^{ext}$ is applied across the film, $\mathbf{H}^{ext} = H_z \mathbf{e}_z = H\mathbf{e}_z$ (H being the magnitude). The units are amperes/meter and in a long solenoid coil, $\mathbf{H}_z\mathbf{e}_z$ would be the number of turns per meter multiplied by the current. There are several alternative terms used for $\mathbf{H}$ (*e.g.*, magnetic intensity vector, but often it is just referred to as 'H'). In any case, it is the magnetic quantity solely dependent on external inputs, rather than properties of the materials, and is thus user-controlled.

When an external field $\mathbf{H}^{ext}$ is applied to a ferromagnetic medium, a magnetization $\mathbf{M}$ occurs. The resulting field $\mathbf{B}$ equals $\mu_0(\mathbf{H} + \mathbf{M})$, but $M \gg H$ so $\mathbf{B}^{ext}$ is essentially equal to $\mu_0 \mathbf{H}^{ext}$. For ferromagnetic materials, the phenomena of saturation and hysteresis occur, see Fig. 4. The vertical axis is essentially the magnetic field B. When an external field H_z is first applied, the ferrous domain becomes magnetized from zero (solid line) eventually attaining a saturation value, M_{sat}. When the field is reduced, the magnetization of the medium follows a different curve (dashed line) with a residual value at $H_z = 0$, *i.e.*, permanent magnetization. If the direction of the field changes, the magnetization curve undergoes a loop (not shown). If $H_z \geq 0$ as in this study, and the applied field is seen to cycle between zero and a positive value at saturation (off/on), the magnetization traverses the dashed line.

In the present preliminary study, a three domain curve-fit to a magnetization curve shown in Fig. 5 is used to model *only* the initial magnetization curve. The curve-fit has the form:

$$\begin{aligned} &M \langle 0.1M_{sat} : M = a_1 H + a_2 H^2 \\ &0.1M_{sat} \leq M \langle 0.95M_{sat} : M = b_0 + b_1 H + b_2 H^2 + b_3 H^3 \\ &M \geq 0.95M_{sat} : M = M_{sat} + c_{-1} H^{-1} \end{aligned} \tag{11}$$

in which the eight constants $M_{sat}, a_1, \ldots, c_{-1}$ are found from experimental data for iron and patching together the three regions. The three-domain procedure and the information from which the parameters are extracted are presented in Ref. [39]. The parameter values are as follows: $M_{sat} = 1.27310^6$ [A/m], $a_1 = 200$ [-], $a_2 = 220$ [m/A], $b_0 = 0.142710^6$ [A/m], $b_1 = 12.3110^3$ [-], $b_2 = 37.96$ [m/A], $b_3 = 0.03965$ [m^2/A^2], and $c_{-1} = 20.4210^6$ [A^2/m^2]. In the above, M represents the magnitude with $\mathbf{M} = M_z\mathbf{e}_z = M\mathbf{e}_z$. It appears that this is the first time such a three-domain magnetization curve has been applied to DEM MR simulations.

The magnetic dipole moment vector of a particle is simply the product of the volume and the magnetization in a uniform field $\mathbf{m} = \mathbf{M}\mathcal{V}_p$. If a magnetic dipole m_j is located at a source point r_j, the field at another point $\mathbf{r}_i$ is given by,

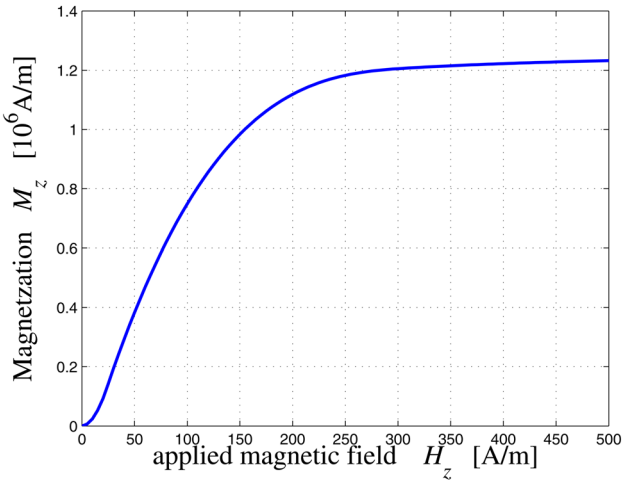

Fig. 5 Magnetization curve used in present model

$$\mathbf{r}' = \mathbf{r}_i - \mathbf{r}_j, \quad \mathbf{e}_i' = \frac{\mathbf{r}'}{|\mathbf{r}'|}, \quad \mathbf{B}(\mathbf{r}_i; \mathbf{r}_j) = \frac{\mu_0}{4\pi}\frac{1}{r'^3}\left(3(\mathbf{m}_j \cdot \mathbf{e}_i')\mathbf{e}_i' - \mathrm{m}_j\right) \tag{12}$$

$$\mathbf{B}(\mathbf{r_i}) = \sum_j^{n_m} \mathbf{B}(\mathbf{r_i}; \mathbf{r_j}) + \mathbf{B}^{ext}, \quad \mathbf{F}_i^m = \nabla(\mathbf{m_i} \cdot \mathbf{B}(\mathbf{r_i})), \quad \mathbf{T}_i^m = \mathbf{m_i} \times \mathbf{B}(\mathbf{r_i}) \tag{13}$$

As in the case of evaluating the mechanical contact forces on a particle, after a small increment of time in the simulations Δt, the updated particle positions may indicate magnetic interaction of particle i with, particles j to n_m, n_m being the number of magnetic 'contacts.' In theory, each particle interacts magnetically with every other particle, but the influence fades rapidly according to the separation distance cubed. For this reason, and with the same concept that is done for interaction forces in molecular dynamics simulations, an effective magnetic radius of six times the actual particle radius is used, $R_m = 6R_p$. The DEM program structure calculates magnetic contact between particles just as it does for physical contact, as described in previous studies. Equations (12) and (13) above are found in many texts on electromagnetics such as Griffths [40].

4 Simulation Results

4.1 Visualizations. The iron MR particle radius used is $R_p = 2\,\mu$m (density $\rho_P = 7500$ kg/m^3), and the wall particle radius

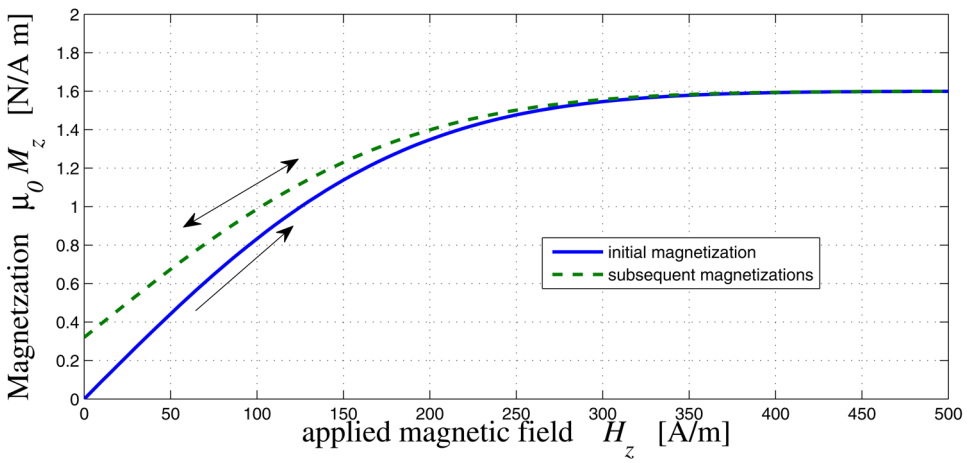

Fig. 4 Typical magnetization curve of a ferro magnetic material

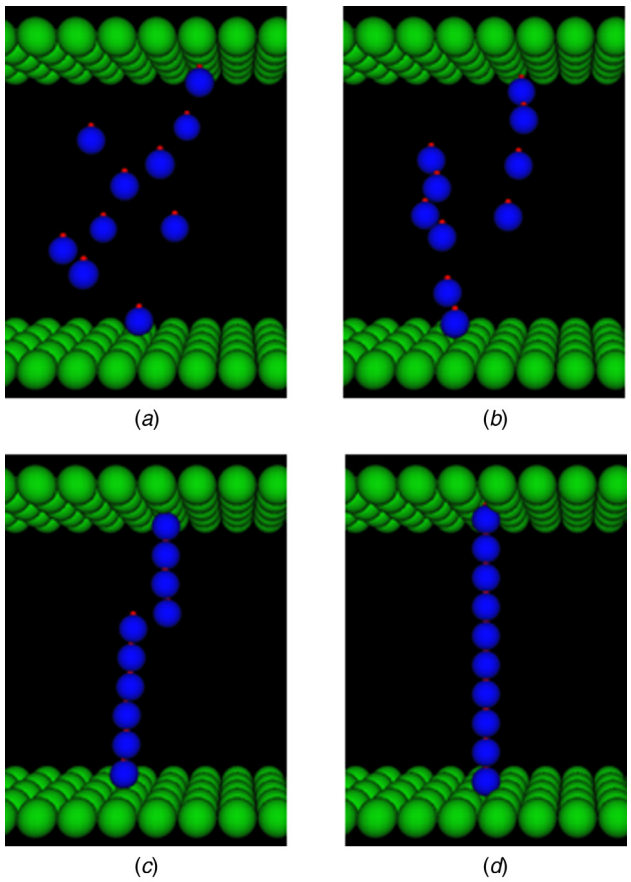

Fig. 6 Alignment of a column of particles in the MR fluid - applied magnetic field with no shear; evolution with time shown from left to right

is $R_\omega = 2.5\ \mu$m. A saturation value of the external magnetic field is used, either 'on' or 'off.' The domain in the direction of sliding is $L_x = 125\ \mu$m (25 wall particles), in the span-wise direction along the film into the plane of the paper $L_y = 25\ \mu$m (5 wall particles). The carrier fluid is assumed to be water, $\eta_f = 1.0$ mPa s, $\rho_f = 1000$ kg/m^3.

In first simulation results portrayed, there are ten particles in the carrier fluid, and in the cross-film direction $L_z = 40\ \mu$m (10 MR particles). The external magnetic field is applied between the two walls and there is no surface shearing motion. Results are close to what is expected: after about $6\mu s$ in simulated time one can see that the particles are aligned vertically, Fig. 6.

Starting from the magnetized state with ten particles aligned, the lower wall starts to move at a velocity of $V_2 = 0.122$ m/s. The shearing results are also close to what is expected - the particle chain inclines to a limit angle around 80° before jumping to the corresponding neighboring location at the wall particles. This change of the angle between the column of particles and the vertical axis corresponds to an increase in force on the upper wall, Fig. 7.

The next image presented is the practical case of shearing velocity $V_x = 0.488$ m/s, film thickness $L_z = 69.6\ \mu$m (about 14 MR particles) in the presence of a saturation magnetic with 28% volume fraction of MR particles. This volume fraction is in the range of industrial applications. The shear rate shown is $\dot{\gamma}_z = 7000\ \text{s}^{-1}$. In this case, the particle column structure is not apparent to the human eye from a given y-plane, although presumably multiple chains are constantly in the process of forming and breaking. The steady mode is reached after 2 10^6 iterations or 50 μs of simulated time (see Fig. 8). If the external magnetic field is suppressed, in the steady mode, the tangential force F_x equals 5.40 10^{-6} N, and the shear stress τ_{zx} equals 1.73 kPa, which gives an off-state viscosity of 0.25 Pa-s. All these results are similar to those of recent experiments [14–16], but conditions are not exactly the same so a direct comparison is not meaningful.

4.2 Predictions of Global Rheological Behavior. Numerous simulations have been performed with the parameters of Figs. 6–8 above - the particle volume fraction is 28%, the domain is $L_z = 125\ \mu$m (25 wall particles), $L_y = 25\ \mu$m (5 wall particles), and $L_z = 69.6\ \mu$m (about 14 MR particles). The particle size and density are those used above, and the simulated viscous fluid has the density and viscosity of water. The surface velocity is varied for the different runs, which has the effect of varying the shear rate. The external applied magnetic field has the value $\mu_0 H_z^{ext} = 0.01$ N/$A \cdot$ m $= 0.01$ T, which has been empirically found to be sufficient to cause saturation in the global behavior, *i.e,* for given conditions, nofurther increase in shear stress is evidenced for an increased applied field. Mean shear stress and shear rate were calculated in the manner described above.

Figure 9 shows some typical behavior of the evolution of shear stress with the number of iterations, which is proportional to simulated time. The magnetic field is applied, and the shear rate is about 10^4 s^{-1}. There are 2×106 iterations, which represent about $50\mu s$ of simulated time. The simulations are time-consuming - a run like that shown takes about five days. Consideration of magnetic force slows the DEM program down considerably, by a factor of 200 or so. In the magnetic case, a given particle interacts with all particles within six times its radius. In the non-magnetic case, a particle only interacts with those with which it actually collides. A data point is captured every 1000 iterations as shown in Fig. 9. Moving averages of the last 100, 250 and 500 data points are shown (averages of the last 10^5, 2.5 10^5, and 5 10^5 iterations, respectively). The data continue to oscillate, but the last

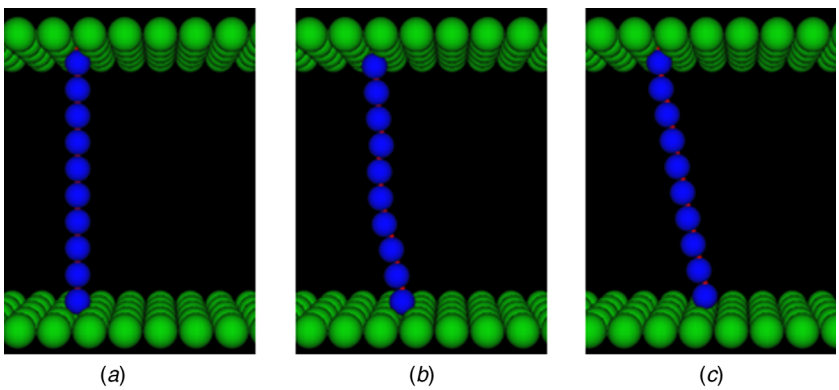

Fig. 7 Shearing of a column of particles in the MR fluid - applied magnetic field; evolution with time shown from left to right

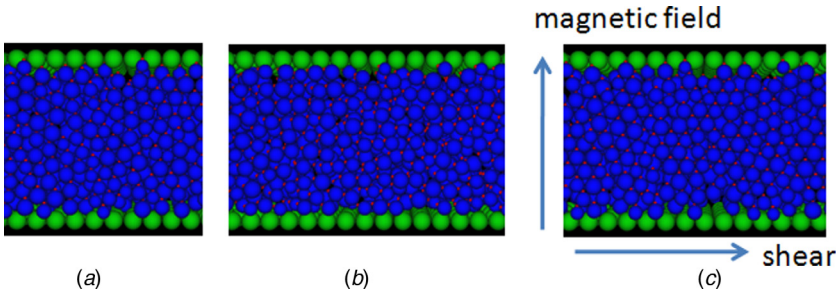

Fig. 8 Shearing of a column of particles in the MR fluid with applied magnetic field

500 moving average is fairly well-behaved. For the results portrayed below, the moving average of the last 500 data points at the 2000th point have been used.

Computed shear stresses have been plotted with and without the external magnetic field in Fig. 10. In the absence of the magnetic field, the fluid is Newtonian: the shear stress is linearly proportional to shear rate and falls to zero in the absence of shearing. The effective viscosity of the mixture is about 0.143 Pa-s: many times greater than water itself (0.001 Pa-s). This indicates that the fluid phase encounters some 140 times greater resistance to flow through the dense ensemble of particles confined between the walls, than to flow between the walls alone. When the magnetic field is applied, results are close to Bingham model in the range shown. The yield shear stress τ_0 in the 'on' mode is about 9.7 kPa, and the viscosity parameter η_0 is about 0.328 Pa-s.

An interesting way to present the current results is in terms of Mason number M_a:

$$\tau^*_{zx} = \frac{\tau_{zx}\left(H_z^{ext}\right)}{\tau_{zx}\left(H_z^{ext}=0\right)}, \quad M\alpha = \frac{\eta_f \dot{\gamma}_{zx}}{\mu_0 \mu_r M_z^2} \tag{14}$$

Mason number [18] is proportional to the ratio of viscous to magnetic forces. There are several alternative versions of Mason number; in particular, the number shown may be preceded by different coefficients. In Eq. (14), a MR fluid relative shear stress is also defined: the shear stress in the 'on' magnetic state divided by shear stress in the 'off' state. When magnetic forces dominate (low Mason number) the on shear stress is about 100 times the off shear stress. At large Mason number, the relative shear stress approaches one. Even with the external field on, the viscous effects overwhelm the magnetic.

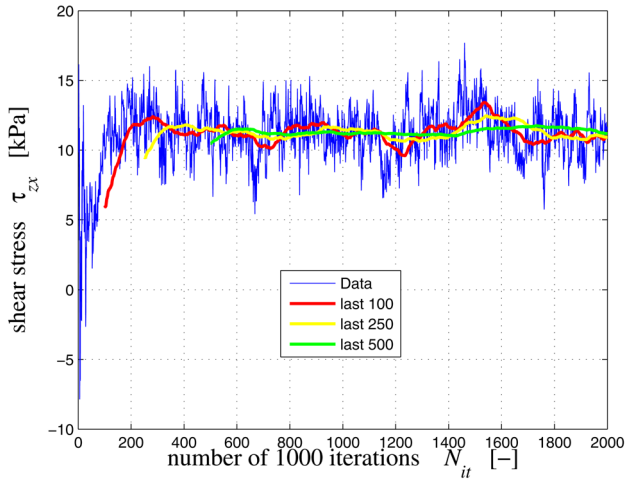

Fig. 9 Simulation results: typical shear stress evolution with time - the behavior of moving averages

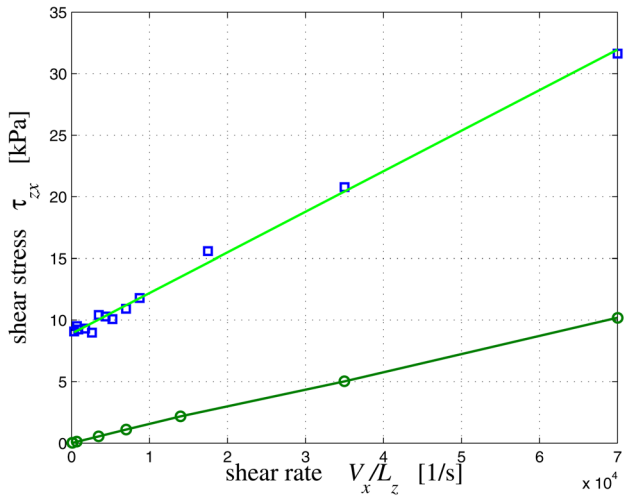

Fig. 10 Simulation results: shear stress versus shear rate - the 'off' condition (no applied magnetic field) is the lower curve, the 'on' condition (applied external magnetic field) is the upper curve

5 Conclusions

This study has shown that the DEM is a useful tool to characterize MR fluids. A discrete element code has been modified to model the magnetic behavior of ferromagnetic particles. A three-domain characterization of the magnetization curve up to saturation has been used. Simulations have shown that MR fluid behavior consistent with that of experiment, has been recovered using this code. As

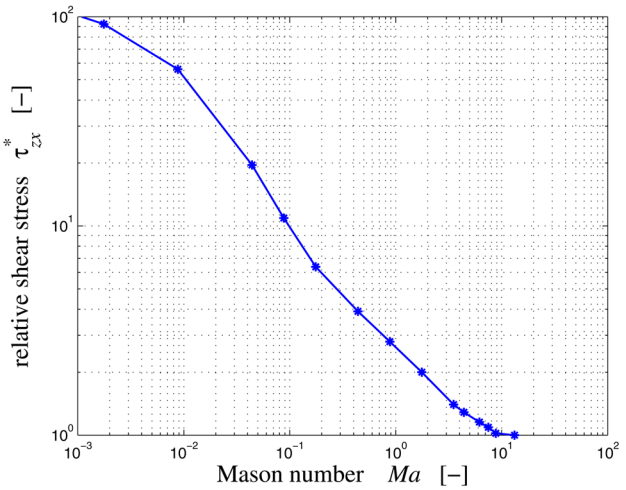

Fig. 11 Simulation results: ratio of 'on' shear stress to 'off' shear stress versus Mason number

observed in real MR fluids, there is a dramatic increase of effective viscosity when an external magnetic field is applied. Moreover, stresses and viscosities in the simulations are in the range of application and experiment which is promising for future use of this simulation technique. An advantage of numerical experiments as those presented herein is that many orders of magnitude of behavior can be treated at one time. Experimental results similar to Fig. 11 appear in the literature, *e.g.*, [14–16] but over a far more limited range of behavior.

Many future uses and improvements of the model are readily envisioned. It would be interesting to describe the magnetization process of particles without neglecting the hysteresis loop and dynamic effects. For further significant advancement (more particles, partial magnetization) an optimization of the code, perhaps through parallelization, would be desirable if not necessary. It would be also interesting to consider the influence of surfactant and additives in order to more accurately simulate commercial MR fluids. Finally, a full coupling of the fluid mechanics of the solvent phase to the particle behavior would be highly desirable, but seems out of reach in the near term.

Nomenclature

$\mathbf{B}=$ magnetic field vector (flux density) N/A · m
$\mathbf{e}=$ unit vector indicating direction -
$E_Y=$ elastic (Young's) Modulus N/m^2
$\mathbf{F}=$ force vector N
$\mathbf{H}=$ magnetic field vector (magnetic intensity, applied field) A/m
$L_x, L_y=$ lengths of domain surface m
$L_z=$ length across domain (film thickness) m
$\mathbf{m}=$ magnetic dipole moment vector N·m^2
$\mathbf{M}=$ magnetization vector A/m
$R=$ radius m
$t=$ time s
$\mathbf{T}=$ Torque (moment) vector N · m
$\mathbf{v}=$ velocity vector m/s
$v_i=$ components component m
$\mathbf{V}=$ surface velocity vector m/s
$\mathbf{x}=$ position vector m
$x_i=$ rectangular coordinate component m
$x, y, z=$ coordinate in sliding direction, spanwise direction, across the film m
$\dot{\gamma}_{kl}=$ rate of strain tensor component, Eq. (1) 1/s
$\dot{\gamma}=$ rate of strain magnitude, Eq. (1) 1/s
$\delta=$ interference (penetration) of particle contact m
$\eta=$ viscosity N · s/m^2
$\eta_0=$ viscosity parameter in Bingham model N · s/m^2
$\mu_0=$ magnetic permeability in a vacuum $= 4\,\pi\,10^{-7}$ N/A^2
$\mu_r=$ relative magnetic permeability, ratio of permeability to vacuum permeability -
$\tau_{ij}=$ extra stress tensor component N/m^2
$\tau=$ stress tensor magnitude, Eq. (1) N/m^2
$\tau_0=$ stress parameter in Bingham model, Eq. (2) N/m^2
$\omega=$ rotation vector 1/s

Subscripts, Superscripts

$f, p=$ fluid, particle
$i, j=$ particle i, particle j
$k, l=$ vector, tensor components
$m, n=$ summation indices
$c, v, m=$ contact, viscous, magnetic
$x, y, z=$ coordinate in sliding direction, spanwise direction, across the film
$n, t=$ normal, tangential

Vector quantities are represented as follows:

$$\mathbf{V}=\sum_{k=1}^{3} V_k\mathbf{e}_k = V_x\mathbf{e}_x + V_y\mathbf{e}_y + V_z\mathbf{e}_z, \quad V=\sqrt{V_x^2+V_y^2+V_z^2}$$

References

[1] Carlson, J. D., and Toscano, J., 2007, "MR Fluids through Thick and Thin," Motion Syst. Des., **49**(6), pp. 52–53.
[2] Ahmadian, M., and Sandu, C., 2008, "An Experimental Evaluation of Magneto-Rheological Front Fork Suspensions for Motorcycle Applications," Int. J. Veh. Syst. Model. Test, **3**(4), pp. 296–311.
[3] Zheng, G., Huang, Y., and Gan, B., 2010, "The Application of MR Fluid Dampers to the Vibrating Screen to Enhance Screening Efficiency," Adv. Mater. Res., **97–101**, pp. 2628–2633.
[4] Huan, R. H., Li, X. P., Wu, Y. J., and Zhu, W. Q., 2010, "Optimal Bounded Semi-Active Control of Hysteretic Systems with MR Damper," Adv. Struct. Eng., **13**(6), pp. 1199–1205.
[5] Kim, E.-S., Choi, S.-B., Park, Y. G., and Lee, S., 2010, "Temperature Control of an Automotive Engine Cooling System Utilizing a Magneto-Rheological Fan Clutch," Smart Mater. Struct., **19**(10), p. 101001.
[6] Nguyen, Q. H., and Choi, S. B., 2010, "Optimal Design of an Automotive Magnetorheological Brake Considering Geometric Dimensions and Zero-Field Friction Heat," Smart Mater. Struct., **19**(11), p. 115024.
[7] Johansson, J. L., Sherrill, D. M., Riley, P. O., Bonato, P., and Herr, H., 2005, "A Clinical Comparison of Variable-Damping and Mechanically Passive Prosthetic Knee Devices," Am. J. Phys. Med. Rehabil., **84**(8), pp. 563–575.
[8] Jonsdottir, F., Thorarinsson, E. W. T., Paisson, H., and Gudmundsson, K. H., 2009, "Influence of Parameter Variations on the Braking Torque of a Magneto-rheological Prosthetic Knee," J. Intell. Mater. Syst. Struct., **20**(6), pp. 659–667.
[9] Herr, H., 2005, "Biohybrid limbs to Restore Arm, Leg function to Amputees," Adv. Mater. Processes, **163**(4), p. 56.
[10] Iordanoff, I., Fillot, N., and Berthier, Y., 2005. "Numerical Study of a Thin Layer of Cohesive Particles under Plane Shearing," Powder Technol., **159**, pp. 46–54.
[11] Fillot, N., Iordanoff, I., and Berthier, Y., 2005, "Simulation of Wear through a Mass Balance," Trans. ASME J. Tribol, **127**(1), pp. 230–237.
[12] Winslow, W. M., 1949, "Induced Fibration of Suspensions," J. Appl. Phys,. **20**, pp. 1137–1140.
[13] Halsey, T., 1992, "Electrorheological Fluids," Science, **258**, pp. 761–766.
[14] Bonnecaze, R. T., and Brady, F., 1992, "Dynamic Simulation of an Electrorheological Fluid," J. Chem. Phys., **96**(3), pp. 2183–2202.
[15] Bonnecaze, R. T., and Brady, F., 1992, "Yield Stresses in Electrorheological Fluids," J. Rheol., **36**(1), pp. 73–115.
[16] Klingenberg, D. J., Swol, F., and Zukoski, C. F., 1989, "Dynamic Simulation of Electrorheological Suspension," J. Chem. Phys., **91**(12), pp. 7688–7895.
[17] Klingenberg, D. J., Swol, F., and Zukoski, C. F., 1991, "The Small Shear Rate Response of Electrorheological Suspension. I. Simulation in the Point-dipole Limit," J. Chem. Phys., **94**(9), pp. 6160–6169.
[18] Klingenberg, D. J., Swol, F., and Zukoski, C. F., 1991, "The Small Shear Rate Response of Electrorheological Suspension. II. Extension Beyond the Point-dipole Limit," J. Chem. Phys., **94**(9), pp. 6170–6178.
[19] Parthasarathy, M., and Klingenberg, D. J., 1999, "Large Amplitude Oscillatory Shear of ER Suspensions," J. Non-Newtonian Fluid Mech., **81**, pp. 83–104.
[20] Chen, T. Y., Briscoe, B. J., and Luckham, P. F., 1995, "Microstructural Studies of Electro-Rheological Fluids under Shear," J. Chem. Soc. Faraday Trans., **91**(12), pp. 1787–1794–104.
[21] Bird, R. B., Armstrong, R. C., and Hassager, O., 1987, *Dynamics of Polymeric Liquids, Fluid Mechanics*. J. Wiley and Sons, New York, Vol. 1.
[22] Tichy, J., 1991, "Hydrodynamic Lubrication Theory for the Bingham Flow Model," J. Rheol., **35**(4), pp. 477–496.
[23] Rankin, P. J., Ginder, J. M., and Klingenberg, D. J.,1998, "Electro- and Magneto-Rheology," Curr. Opin. Colloid Interface Sci., **3**(4), pp. 373–381.
[24] de Vicente, J., López-López, M. T., Durán, J. D. G., and González-Caballero, F., 2004, "Shear Flow Behavior of Confined Magnetorheological Fluids at Low Magnetic Field Strengths," Rheol. Acta, **44**, pp. 94–103.
[25] Genç, S., and Phulé, P. P., 2002, "Rheological Properties of Magnetorheological Fluids," Smart Mater. Struct., **11**, pp. 140–146.
[26] Klingenberg, D. J., Olk, C. H., Golden, M. A., and Ulicny, J. C., 2010, "Effects of Nonmagnetic Interparticle Forces on Magnetorheological Fluids," J. Phys.: Condens. Matter, **22**, p. 324101.
[27] Claracq, J., Sarrazin, J., and Monfort, J., 2004, "Viscoelastic Properties of Magnetorheological Fluids," Rheol. Acta, **43**, pp. 38–49.
[28] Bird, R. B., Curtiss, C., Armstrong, R. C., and Hassager, O., 1987, *Dynamics of Polymeric Liquids, Vol. 2: Kinetic Theory*, J. Wiley and Sons, New York.
[29] Larson, R. G., 1999, *The Structure and Rheology of Complex Fluids*, Oxford Press, New York.
[30] Yi, C., Peng, X., and Zhao, C., 2010,"A Magnetic-Dipoles-Based Micro-Macro Constitutive Model for MRFs subjected to Shear Deformation," Rheol. Acta, **49**, pp. 815–825.
[31] Furst, E. M., and Gast, A. P., 2000, "Micromechanics of Magnetorheological Suspensions," Phys. Rev. E, **61**(6), pp. 6732–6739.
[32] Jang, K.-I., Seok, J., Min, B.-K., and Lee, S. J., 2009, "Behavioral Model for Magnetorheological Fluid under a Magnetic Field using Lekner Summation Method," J. Magn. Magn. Mater., **321**, pp. 1167–1176.
[33] Ginder, J. M., and Davis, L. C., 1994, "Shear Stresses in Magnetorheological Fluids: Role of Magnetic Saturation," Appl. Phys. Lett., **26**, pp. 3410–3412.
[34] Kroger, M., Ilg, P., and Hess, S., 2003, "Magnetoviscous Model Fluids," J. Phys. Condens. Matter, **15**(15), pp. S1403–S1423.
[35] Han, K., Feng, Y. T., and Owen, D. R. J., 2010, "Three-Dimensional Modeling and Simulation of Magnetorheological Fluids," Int. J. Numer. Methods Eng., **84**(11), pp. 1273–1302.

[36] Melle, S., Calderón, O. G., Rubio, M. A., and Fuller, G. G., 2003, "Microstructure Evolution in Magnetorheological Suspensions Governed by Mason Number," Phys. Rev. E, **68**(11), p. 041503.
[37] Allen, M. P., and Tildesley, D. J., 1987, *Computer Simulation of Liquids*, Oxford Science Publications, Oxford.
[38] Happel, J., and Brenner, H., 1973, *Low Reynolds Number Hydrodynamics*, Noordhoff International, Leyden.
[39] du Trémolet de Lacheisserie, E., 1999, *Magnétisme*, Grenoble Sciences, Grenoble.
[40] Griffiths, D., 1989, *Introduction to Electrodynamics*, Prentice-Hall, Englewood Cliffs NJ.